Journal of Medicinal Chemistry

pubs.acs.org/jmc Article

Tricyclic-Carbocyclic RORγt Inverse Agonists—Discovery of BMS-986313

Michael G. Yang,* Myra Beaudoin-Bertrand, Zili Xiao, David Marcoux, Carolyn A. Weigelt, Shiuhang Yip, Dauh-Rurng Wu, Max Ruzanov, John S. Sack, Jinhong Wang, Melissa Yarde, Sha Li, David J. Shuster, Jenny H. Xie, Tara Sherry, Mary T. Obermeier, Aberra Fura, Kevin Stefanski, Georgia Cornelius, Purnima Khandelwal, Ananta Karmakar, Mushkin Basha, Venkatesh Babu, Arun Kumar Gupta, Arvind Mathur, Luisa Salter-Cid, Rex Denton, Qihong Zhao, and T. G. Murali Dhar*

Cite This: J. Med. Chem. 2021, 64, 2714−2724 Read Online

ACCESS | Metrics & More | Article Recommendations | Supporting Information

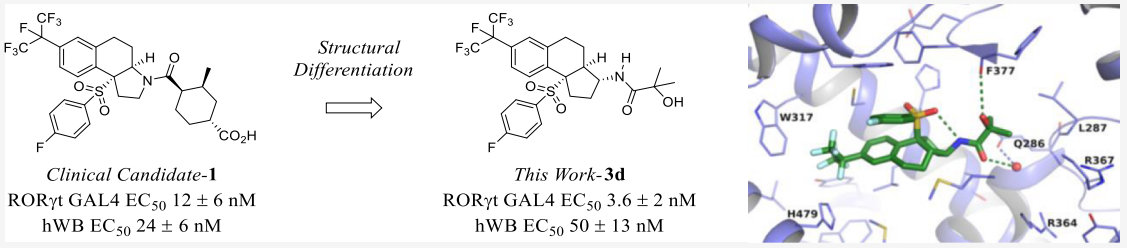

ABSTRACT: SAR efforts directed at identifying RORγt inverse agonists structurally different from our clinical compound **1** (BMS-986251) led to tricyclic-carbocyclic analogues represented by **3**−**7** and culminated in the identification of **3d** (BMS-986313), with structural differences distinct from **1**. The X-ray co-crystal structure of **3d** with the ligand binding domain of RORγt revealed several key interactions, which are different from **1**. The in vitro and in vivo PK profiles of **3d** are described. In addition, we demonstrate robust efficacy of **3d** in two preclinical models of psoriasis—the IMQ-induced skin lesion model and the IL-23-induced acanthosis model. The efficacy seen with **3d** in these models is comparable to the results observed with **1**.

INTRODUCTION

The retinoid-related orphan receptor (ROR) is a member of the nuclear hormone receptor family and consists of RORα, β, and γ subfamilies. RORγt is a shorter isoform of RORγ, differing by 24 amino acids at the *N*-terminal extension.[1] Unlike RORγ,[2] the expression of RORγt is restricted primarily to lymphoid cells.[3] RORγt is associated with the regulation of $CD4^+$ T cell differentiation into T helper 17 (T_H17) cells through cytokine signaling pathways including IL-17A/F and IL-23.[4] The activation of RORγt upregulates the expressions of IL-23R, T_H17 cells, and the production of pro-inflammatory cytokines, such as IL-17A/F, IL-22, IL-26, and CCL20.[5] Studies have shown that the overproduction of these pro-inflammatory cytokines is linked to several human autoimmune disorders such as psoriasis.[6] This approach has been validated in the clinic by marketed antibodies targeting IL-17 (secukinumab, ixekizumab), its receptor (brodalumab), and the IL-23 p19 subunit (guselkumab), for the treatment of psoriasis, ankylosing spondylitis, and active psoriatic arthritis.[7,8] In addition, clinical proof-of-concept (PoC) with small molecule inverse agonists of RORγt has been achieved with VTP-43742 for the treatment of psoriasis,[9] and pre-clinical PoC for this mechanism has also been established for the treatment of inflammatory bowel disease, rheumatoid arthritis, and other autoimmune diseases.[10−13]

In light of these findings, there has been significant interest in academic institutions and pharmaceutical companies to identify small molecule inverse agonists of RORγt.[14−19] Recently, we reported the discovery of **1** and **2** as potent and selective RORγt inverse agonists.[20−23] Although compound **2** was structurally differentiated from **1**, the metabolic stability (MetStab) profile was not optimal, and this prevented its further development (Figure 1).[22] In addition, for our second generation series, we elected to stay away from acid moieties (as in **1**) because of the potential liabilities associated with acyl glucuronide formation. Therefore, efforts to prepare RORγt inverse agonists with an improved MetStab profile over

Received: November 17, 2020
Published: February 16, 2021

https://dx.doi.org/10.1021/acs.jmedchem.0c01992
J. Med. Chem. 2021, 64, 2714−2724

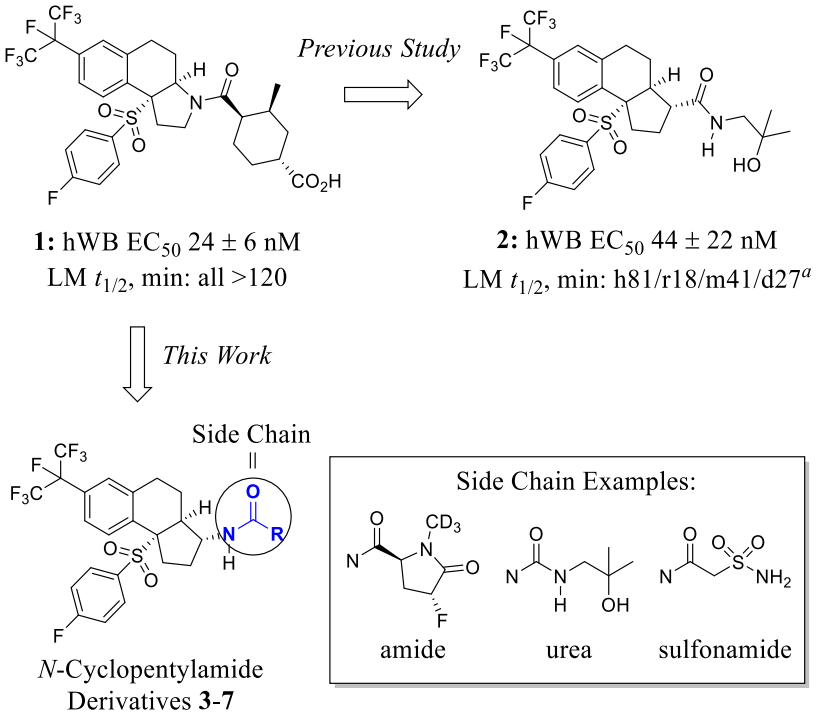

Figure 1. Development of orally bioavailable RORγt inverse agonists **3**–**7**. [a]LM $t_{1/2}$: liver microsomes half-life in minutes, human (h), rat (r), mouse (m), and dog (d).

Table 1. SAR Study of the Side Chains Presented in Molecules 3–7[a]

Side Chain Modifications:

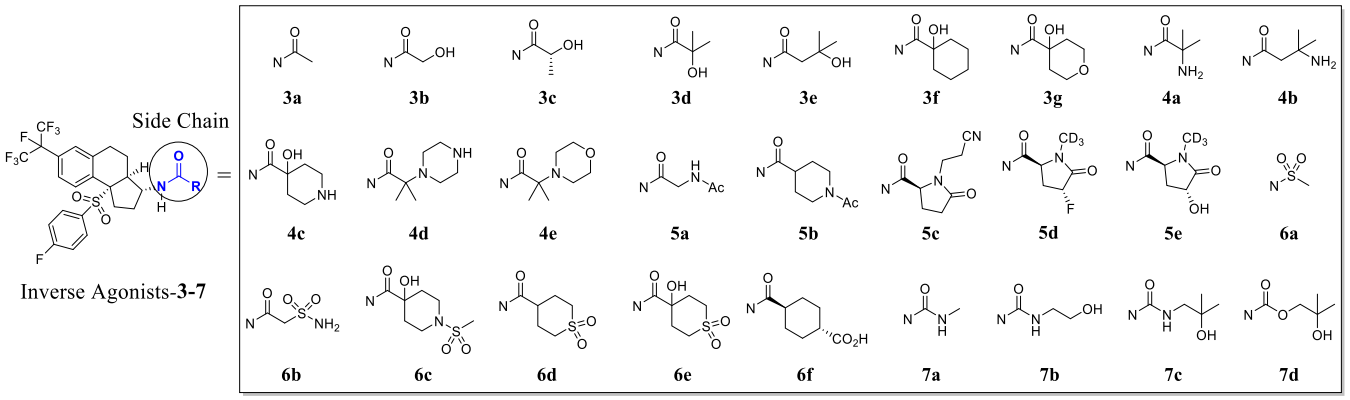

compd	RORγt GAL4 EC_{50} (nM)	IL-17 hWB EC_{50} (nM)[a]	MetStab % rem (h/m/r)[b]	compd	RORγt GAL4 EC_{50} (nM)	IL-17 hWB EC_{50} (nM)[a]	MetStab % rem (h/m/r)[b]
3a	5.4	120 ± 16	ND[c]/90/100	**5c**	20	96 ± 29	ND/71/99
3b	8.5	116 ± 21	82/65/34	**5d**	5.4	48 ± 29	100/86/100
3c	8.6	64 ± 32	71/70/14	**5e**	12.3	134 ± 22	99/100/100
3d	3.6	50 ± 13	100/92/100	**6a**	7.3	157 ± 48	ND
3e	2.5	54 ± 20	97/86/90	**6b**	9.9	127 ± 36	ND
3f	1.4	67 ± 31	50/56/22	**6c**	6.7	28 ± 13	97/100/100
3g	7.4	21 ± 5	100/75/66	**6d**	8.7	50 ± 24	100/95/100
4a	30	164 ± 11	80/100/100	**6e**	1.9	36 ± 17	97/99/97
4b	48	981 ± 223	98/85/89	**6f**	24	291	100/100/100
4c	26	1940	100/88/83	**7a**	3.7	101 ± 67	40/32/10
4d	63	ND	74/78/97	**7b**	2.5	65 ± 28	97/93/41
4e	2.2	39 ± 5	0.3/0.3/0.4	**7c**	3.1	32 ± 2	54/ND/42
5a	4.5	95 ± 63	100/93/10	**7d**	9.1	91 ± 8	ND
5b	15	34 ± 10	61/67/100	**1**	12	24 ± 6	100/100/100

[a]EC_{50} values reported as the average of two or more determinations. [b]In vitro stability in the human (h), mouse (m), and rat (r) liver microsomes. [c]Not determined.

https://dx.doi.org/10.1021/acs.jmedchem.0c01992
J. Med. Chem. 2021, 64, 2714−2724

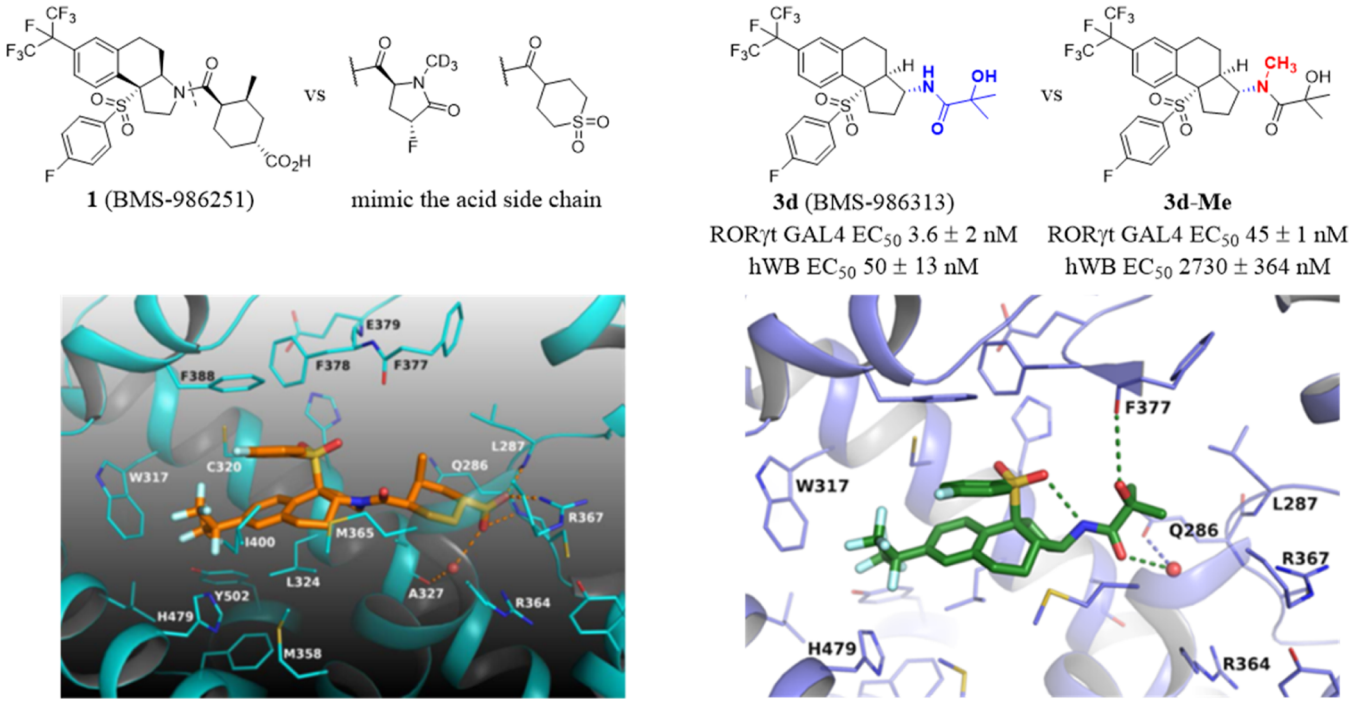

Figure 2. Left panel: X-ray co-crystal structure of **1** (BMS-986251) in RORγt (pdb id: 6VQF); right panel: co-crystal structure of **3d** (BMS-986313) with the LBD of RORγt (pdb id: 7KQJ).

2 led to the identification of tricyclic *N*-cyclopentyl-derived analogues **3**−**7** (Figure 1). This manuscript details the SAR findings of **3**−**7** and reports the in vivo results of **3d** in two preclinical models of psoriasis: the imiquimod (IMQ)-induced skin lesion model and IL-23-induced acanthosis model of psoriasis.

RESULTS AND DISCUSSION

Efforts aimed at improving the MetStab profile of **2** led to the examination of a series of reverse amides **3**−**7**, as listed in Table 1. Compared to structure **2** (Figure 1), the side chain amide nitrogen in the new series (compounds **3**−**7**) is sterically hindered because it is attached to the tricyclic core, which could potentially alter or slow down metabolic processes such as N-dealkylation. Because the reverse amide series was a logical extension from our earlier tricyclic pyrrolidine series where the nitrogen atom was a part of the ring system, as illustrated in **1**,[20,21] a number of side chains studied earlier were re-examined here. Molecular modeling studies revealed that the trajectory of the side chains in both tricyclic pyrrolidine and reverse amide series point toward the RORγt polar pocket, consisting of a network of residues including Glu286, Leu287, Arg364, and Arg367.

As part of the screening process, we tested all newly synthesized compounds in both the GaL4-Luc reporter assay (GAL4) and a physiologically relevant IL-17-stimulated human whole blood (hWB) assay. Because the hWB EC_{50} of **1** was 24 nM,[21] we required the EC_{50} cutoff value of newly synthesized compounds to be ≤50 nM for further profiling. To assess MetStab, we measured the percent of parent remaining (% rem) following incubation with human, mouse, and rat liver microsomes, aiming for >90% recovery in these assays (Table 1).[24] These results are outlined in Table 1. Acetamide **3a** showed weak hWB activity (EC_{50} = 120 nM) but had good in vitro MetStab in rodents relative to **2**. Next, we examined a group of polar amide analogues directed at engaging the polar pocket of the ligand binding domain (LBD) of RORγt. Among the alcohol derivatives **3b**−**g**, compound **3g** had the best hWB potency (EC_{50} = 21 nM). However, only the tertiary alcohol **3d** met the progression criteria [hWB EC_{50} = 50 nM and MetStab % rem (h/r/m) = 100/92/100]. It is worth noting that α-methyl substituents in **3c** and **3d** showed a trend toward improvement in the hWB potency, as illustrated in Table 1. Amine analogues **4a**−**e** were generally weak in both the GAL4 and hWB assays, except **4e** (hWB EC_{50} = 39 nM). However, the MetStab profile of **4e** was very poor [MetStab % rem (h/r/m) = 0.3/0.3/0.4]. Among the amide analogues **5a** to **5e**, only **5b** and **5d** met the hWB criteria for progression. In addition, **5d** exhibited good MetStab. Next, we examined a series of sulfone and sulfonamide analogues **6a**−**e**, as well as compound **6f** as a representative carboxylic acid. Both **6a** and **6b** had a weak hWB potency (EC_{50} > 120 nM). On the other hand, compounds **6c**−**e** were very potent in the hWB assay with good MetStab, meeting the hWB and in vitro MetStab progression criteria. It was somewhat surprising to see carboxylic acid **6f** to be ∼ 12- to 8-fold less potent than **6e** in the GAL4 and hWB assays, respectively. In the case of our previously reported tricyclic pyrrolidine chemotype,[20] the difference in potency in the GAL4 and hWB assays was only 2−3 fold, suggesting a potentially different binding mode for the sulfone and the carboxylic acid moieties in this chemotype. Ureas **7a**−**c** gave moderate to good potency in the hWB assay, with **7c** affording the best EC_{50} value of 32 nM. Compared to urea **7c**, carbamate **7d** reduced the whole blood activity by 3-fold (**7c**: EC_{50} = 32 nM vs **7d**: EC_{50} = 91 nM). Unfortunately, **7c** had poor MetStab in the in vitro microsomal assays which prevented its further progression.

Based on the activity profiles of compounds in the GAL4 and hWB assays and the in vitro liver microsomal data (Table 1), compounds **3d**, **5d**, and **6c**−**e** were advanced for further

https://dx.doi.org/10.1021/acs.jmedchem.0c01992
J. Med. Chem. 2021, 64, 2714−2724

profiling. The potency of **5d** and **6c−e** can be rationalized based on information obtained from the X-ray co-crystal structure of **1** with the LBD of RORγt (Figure 2, left panel).[21] As shown in Figure 2, the acid moiety of **1** binds in the polar pocket of RORγt and forms hydrogen bonds with the backbone NH of Leu287 and Gln286 and with the side chain of Arg367 and the backbone carbonyl of Ala327 via water. In the design of **5d** and **6c−e**, it was our intention to mimic the carboxylic acid moiety of **1** with the pyrrolidinone[23] and sulfone motifs[20] to achieve the desired interactions. The potencies of **5d** and **6c−e** can potentially be explained based on this rationale. However, we did not expect to see the potent GAL4 and hWB activity for **3d** ($EC_{50's}$ of 3.6 and 50 nM, respectively) because the 2-hydroxy-2-methylpropanamide side chain is too short to fully extend into the polar pocket of RORγt. In an effort to understand the observed potency, the X-ray co-crystal structure of **3d** with the LBD of RORγt was acquired (Figure 2, right panel). Three things became evident from the co-crystal structure: (1) the aryl sulfone forms an intramolecular H-bond with the cyclopentylacetamide NH; (2) the OH moiety of the 2-hydroxy-2-methylpropanamide side chain forms hydrogen bonds with the C═O of Phe377; and (3) the C═O group in the 2-hydroxy-2-methylpropanamide side chain interacts with the backbone carbonyl of Gln286 through water. In addition, the α,α-dimethyl substituents in **3d** likely engages in lipophilic interactions with the side chains of Gln286, Leu287, and Ala368 in the RORγt LBD pocket. Taken together, these interactions probably contribute to the potency enhancements seen with compounds like **3d**. It is worth mentioning that the intramolecular H-bond between the amide NH and the sulfone oxygen is likely the key interaction that preorganizes the side chain of the molecule in the desired orientation to engage in the important interactions described above. The significant loss of potency observed with the N−Me analogue (**3d-Me**, Figure 2) in both the Gal4 and hWB assays is consistent with this hypothesis.

Table 2 summarizes the liver microsome half-life (LM $t_{1/2}$) and Caco-2 data for **3d**, **5d**, **6c−e**, and **1**. Based on the overall

Table 2. In Vitro Characterizations of RORγt Inverse Agonist 3d, 5d, and 6c−e

compd	IL-17 hWB EC_{50} (nM)[a]	LM $t_{1/2}$ (min)[b] h, m, r, d, c	Caco-2 Pc, nm/s (efflux ratio)
3d	50 ± 13	120, 120, 120, 120, 120	106 (0.5)
5d	48 ± 29	46, 38, 56, 120, 24	92 (0.7)
6c	28 ± 13	120, 120, 89, 120, 65	53 (1.4)
6d	50 ± 24	101, 120, 120, 120, 120	73 (1.4)
6e	36 ± 17	120, 120, 120, 120, 120	46 (2.6)
1	24 ± 6	120, 120, 120, 120, 120	240 (0.5)

[a]IC_{50} values reported as the average of two or more determinations. [b]Liver microsomes half-life in minutes.

profiles shown in Table 2, **3d** and **6e** became compounds of interest. Of the two compounds, **3d** was chosen for further advancement based on its potency in the hWB assay, higher Caco-2 value (A−B: 106 nm/s), lower efflux ratio (0.5), and the desired in vitro MetStab profile across species. In addition, the examination of results from mouse coarse PK studies of **3d** and **6e** (orally dosed at 4 mg/kg) clearly indicated that **3d** had a higher oral exposure in terms of both C_{max} (1.04 μM) and area under the curve (AUC_{0-24h}) (15.4 μM·h) compared to **6e** (C_{max} 0.77 μM and AUC_{0-24h} 11.1 μM·h). Therefore, **3d** was advanced for additional in vitro profiling and full PK studies in mouse, rat, dog, and cyno.

In vitro liability profiling results for **3d** are summarized in Table 3. Compound **3d** displayed excellent selectivity against

Table 3. In Vitro Profiling of Compound 3d

parameter	3d	1
RORγt GAL4 EC_{50} (nM)	3.6 ± 2.3	12 ± 6
IL-17 hWB EC_{50} (nM)	50 ± 13	24 ± 6
mouse Th17 EC_{50} (nM)	2.7 ± 0.3	11 ± 2
RORα GAL4 EC_{50} (nM)	>10,000	>10,000
RORβ GAL4 EC_{50} (nM)	>10,000	>10,000
PXR/LXR_{α}/LXR_{β}[a] EC_{50} (nM)	all >5,000	all >5,000
hERG patch clamp IC_{50} (μM):	19	>30
protein binding % free (h &; m):	0.5/0.6	1.2/1.6
CYP[b] inhibition IC_{50} (μM)		
1A2/2D6/2C9	20/20/12	20/20/20
3A4/2C8/2C19	11/12/19	20/16/20

[a]PXR = pregnane X receptor; LXR = liver X receptor. [b]CYP = cytochrome P450.

RORα, RORβ, LXRα/β, and PXR, as well as a favorable IC_{50} in the hERG patch clamp assay and a clean CYP inhibition profile (IC_{50} = 10−20 μM). As listed in Table 4, compound **3d** displays good oral bioavailability (65−100%) across the four species studied, in addition to exhibiting low clearance, consistent with the in vitro liver microsomal $t_{1/2}$. The oral exposures of **3d** (both C_{max} and AUC_{0-24h}) were good across species and were consistent with the permeability suggested by the in vitro Caco-2 assay.

The efficacy of **3d** in chronic disease models was assessed in both the IMQ-induced skin lesion model and the IL-23-induced acanthosis model of psoriasis (Figures 3 and 4). IMQ activates pro-inflammatory signaling pathways and contributes to the induction of clinical signs of psoriasis, such as skin thickening. Skin thickness scores (% change) were measured and recorded daily throughout the 8 day study. Doses of **3d** at 5, 10 and 20 mg/kg BID inhibited skin thickening by 13.7, 39.6, and 57.7%, respectively, compared to the placebo arm based on the area under the curve over the duration of the study. In comparison, the αIL-23 mAb used as a positive control inhibited skin thickening by 65% when dosed at 10 mg/kg (Figure 3B). At the end of the study, the skin was collected and mRNA extracted for RT-PCR analysis. As shown in Figure 3C, both IL-17A and IL-17F mRNA levels were significantly reduced by compound **3d**. At the 10 mg/kg dose, the inhibition of IL-17A and IL-17F by **3d** was comparable to the results observed with the αIL-23 mAb.

Activation of IL-23R promotes the development of Th17 cells and the resulting production of cytokines such as IL-17A and IL-17F, which are involved in mediating psoriasiform changes. The IL-23-induced psoriasis model involves the injection of IL-23 into the ear of C57BL/6 mice, which contributes to the development of dermal inflammation and epidermal hyperplasia (acanthosis). A starting "baseline" measurement of the ear was made on day 0, and ear thickness (% change) was measured every other day prior to the next ear injection. In the IL-23-induced acanthosis study of **3d**, all the

https://dx.doi.org/10.1021/acs.jmedchem.0c01992
J. Med. Chem. 2021, 64, 2714−2724

Table 4. PK Profile of Compound 3d in Preclinical Species[a]

		IV		PO		
species	dose (mg/kg) IV/PO	Cl (mL/min/kg)	V_{ss} (L/kg)	C_{max} (μM)	AUC_{24h} (μM·h)	F (%)
mouse	2/4 (2/4)[b]	3.7 (2.7)	3.0 (1.9)	2.2 (4.8)	33.2 (37)	100 (100)
rat	2/4 (2/4)	4.2 (1.3)	2.9 (1.2)	1.0 (4.7)	17.0 (64)	65 (94)
dog	1/2 (1/1)	0.8 (0.2)	3.2 (0.5)	1.3 (6.4)	59.8 (120)	83 (100)
cyno	1/2 (1/1)	2.7 (1.1)	2.7 (2.0)	1.1 (3.1)	18.0 (35)	75 (100)

[a]Values are means obtained from three or more animals. [b]Data in parenthesis are the PK data for compound **1**.

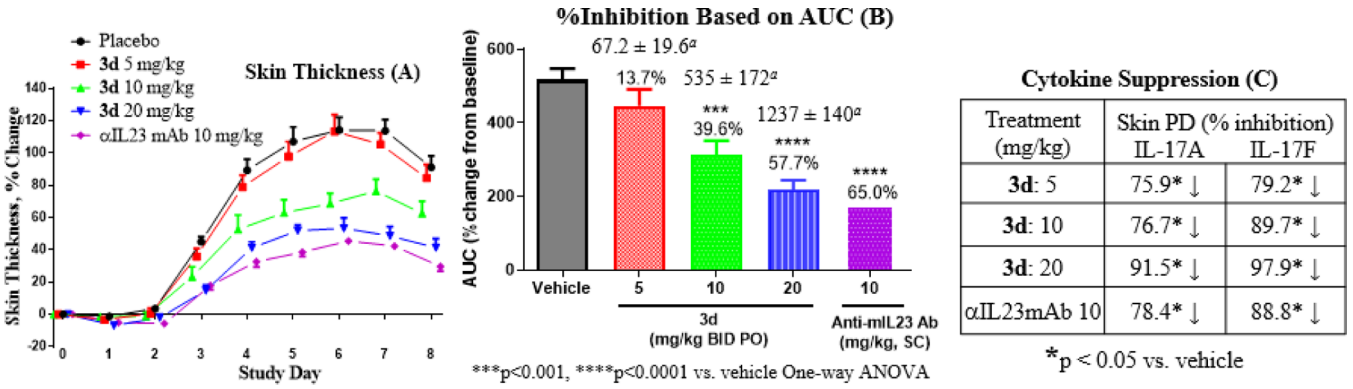

Figure 3. Efficacy of **3d** in an IMQ mouse model: (A) % change in skin thickness scores; (B) % inhibition of skin thickness based on AUC; and (C) % inhibition of IL-17A and IL-17F. [a]Steady-state (SS) exposures, C_{24h}.

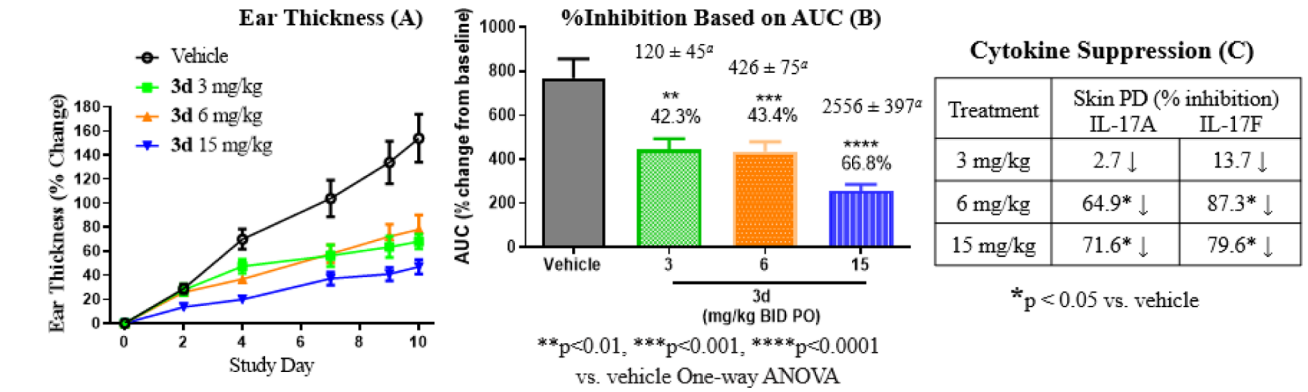

Figure 4. Efficacy of **3d** in an IL-23-induced mouse acanthosis model: (A) % change in ear thickness cores; (B) % inhibition of ear thickness based on AUC; and (C) % inhibition of IL-17A and IL-17F. [a]Steady-state (SS) exposures, C_{24h}.

Scheme 1. Synthesis of Compound 5d[a]

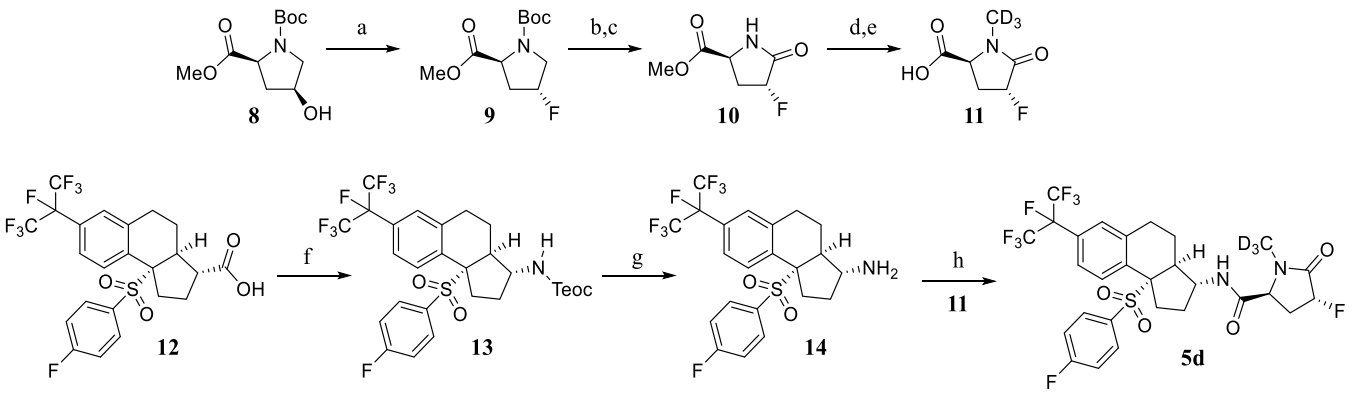

[a]Reagents and conditions: (a) DAST and CH_2Cl_2, 0 °C → rt, 94%; (b) $RuO_2·H_2O$, $NaIO_4$, and EtOAc−H_2O, rt, 63%; (c) 4 M HCl in dioxane and DCM, rt, 81%; (d) Cs_2CO_3, ICD_3, and MeCN, 45 °C → rt, ∼100%, crude used as such for next step; (e) LiOH and THF/MeOH/H_2O, rt, crude used as such for the next step; (f) TEA, toluene, and DPPA, 0 °C → rt, and then heated at 80 °C with $TMSCH_2CH_2OH$; (g) TFA and CH_2Cl_2, rt, 28% over two steps; and (h) HATU, DIEA, and DMF, rt, 53%.

https://dx.doi.org/10.1021/acs.jmedchem.0c01992
J. Med. Chem. 2021, 64, 2714−2724

doses resulted in reduced ear thickness, as shown in Figure 4A. Doses of 3, 6, and 15 mg/kg BID inhibited IL-23-induced ear thickening by 42.3, 43.4, and 66.8%, respectively, compared to the placebo arm based on the area under the curve over the duration of the study (Figure 4B). At the end of the study on day 10, the ear tissue was collected from all animals and analyzed by qPCR for the expression of inflammatory cytokine genes, such as IL-17A and IL-17F. As shown in Figure 4C, compound **3d** provided a dose-dependent inhibition in the levels of IL-17A and IL-17F mRNAs in the ear tissue. These reductions were statistically significant for the 6 and 15 mg/kg doses. The results presented in Figures 3 and 4 show that **3d** demonstrates compelling efficacy in both preclinical models of psoriasis, consistent with its in vitro profile.

CHEMISTRY

As a representative example for the preparation of **3**−**7**, the synthesis of **5d** is outlined in Scheme 1. The DAST reaction of **8** led to the inversion of the configuration at the carbon bearing the hydroxyl group to provide fluoro compound **9** in 94% yield. Ruthenium oxide-catalyzed oxidation of **9** followed by deprotection of the Boc group yielded **10**. Deuteromethylation of **10** followed by saponification gave acid **11**.[23,25] DPPA-promoted Curtis rearrangement reaction of **12**[22] gave tricyclic core **13**, the Teoc group of which was deprotected with TFA to give amine **14** in 28% yield over two steps.[22,25] Finally, the HATU-promoted coupling reaction between acid **11** and amine **14** provided **5d** in 53% yield (Scheme 1).

CONCLUSIONS

Our effort to identify potent, selective, and orally bioavailable RORγt inverse agonists led to the discovery of clinical compound **1**. With the goal of preparing RORγt inverse agonists structurally different from **1**, SAR studies of tricyclic *N*-cyclopentylamide-derived **3**−**7** were conducted, which led to the identification of BMS-986313 (**3d**). Compound **3d** in addition to being structurally different from **1**, also displayed differential and distinct interactions with the LBD of RORγt, as is evident from the X-ray co-crystal structures. **3d** has a clean liability profile and showed excellent PK in multiple preclinical species. Furthermore, **3d** was evaluated in two preclinical models of psoriasis, the IMQ-induced skin lesion model and the IL-23-induced acanthosis model, where it showed robust efficacy comparable to that of an antibody (αIL-23 mAb), thereby warranting further evaluation.

EXPERIMENTAL SECTION

Chemistry. All commercially available chemicals and solvents were used without further purification. Reactions are performed under an atmosphere of nitrogen. All new compounds gave satisfactory ^{1}H nuclear magnetic resonance spectroscopy (NMR), liquid chromatography/mass spectrometry and/or high-resolution mass spectrometry, and mass spectrometry results. ^{1}H NMR spectra were obtained on a Bruker 400 MHz or a Jeol 500 MHz NMR spectrometer using the residual signal of the deuterated NMR solvent as an internal reference. Electrospray ionization (ESI) mass spectra were obtained on a Water Micromass ESI-MS single quadrupole mass spectrometer. The purity of the tested compounds determined by analytical HPLC was >95% except as noted. The analytical HPLC conditions (except as noted) are described as: Waters XBridge C18, 2.1 mm × 50 mm, 1.7 μm particles; mobile phase A: 5:95 acetonitrile/water with 10 mM ammonium acetate; mobile phase B: 95:5 acetonitrile/water with 10 mM ammonium acetate; gradient: 0% B to 100% B over 3 min, then a 0.75 min hold at 100% B; and flow rate: 1 mL/min.

***N*-((3*R*,3a*S*,9b*S*)-9b-((4-Fluorophenyl)sulfonyl)-7-(perfluoropropan-2-yl)-2,3,3a,4,5,9b-hexahydro-1*H*-cyclopenta[*a*]naphthalen-3-yl)acetamide (3a, Table 1).** To a solution of **14** (40 mg, 0.078 mmol; see ref 25. for its synthesis) in CH_2Cl_2 (2 mL) was treated with acetyl chloride (7.95 mg, 0.101 mmol) and triethylamine (10.86 μL, 0.078 mmol) at rt and stirred at rt for 2 h. The reaction mixture was diluted with water (10 mL), extracted with ethyl acetate (10 × 2 mL) and the combined ethyl acetate extracts were dried over Na_2SO_4 and concentrated under rotary evaporation. The crude material was purified by preparative HPLC [Xbridge C18 19 × 200 mm, 5 μm (Waters Corp.); mobile phase A: 5:95 MeCN/water with 10 mM ammonium acetate; mobile phase B: 95:5 MeCN/water with 10 mM ammonium acetate; flow rate 20 mL/min; gradient: increasing B, then isocratic at 100% B] to give **3a** (21.2 mg, 49% yield). ^{1}H NMR (500 MHz, DMSO-d_6): δ 8.11 (br d, *J* = 7.6 Hz, 1H), 7.52−7.44 (m, 2H), 7.36 (s, 1H), 7.33−7.25 (m, 4H), 4.06−3.86 (m, 1H), 3.08−2.92 (m, 1H), 2.80 (br d, *J* = 5.8 Hz, 1H), 2.71−2.60 (m, 1H), 2.32−2.15 (m, 1H), 2.08−1.91 (m, 3H), 1.89−1.79 (m, 4H), 1.35−1.22 (m, 2H). ESI-MS: *m*/*z* 556.18 ([M + H$^+$]). HPLC: t_R = 2.17 min.

***N*-((3*R*,3a*S*,9b*S*)-9b-((4-Fluorophenyl)sulfonyl)-7-(perfluoropropan-2-yl)-2,3,3a,4,5,9b-hexahydro-1*H*-cyclopenta[*a*]naphthalen-3-yl)-2-hydroxyacetamide (3b, Table 1).** To a solution of **14** (26 mg, 0.042 mmol) in DMF (1 mL) was treated with 2-hydroxyacetic acid (14.24 mg, 0.173 mmol), DIEA (0.096 mL, 0.549 mmol), and HATU (48.1 mg, 0.127 mmol). The reaction mixture was stirred at rt for 30 min before water (10 mL) was added. The resulting mixture was extracted with ethyl acetate (10 × 2 mL), and the combined ethyl acetate extracts were dried over Na_2SO_4 and concentrated under rotary evaporation. The crude material was purified by preparative HPLC [Xbridge C18 19 × 200 mm, 5 μm (Waters Corp.); mobile phase A: 5:95 MeCN/water with 10 mM ammonium acetate; mobile phase B: 95:5 MeCN/water with 10 mM ammonium acetate; flow rate 20 mL/min; gradient: increasing B, then isocratic at 100% B] to give **3b** (19.6 mg, 81% yield). ^{1}H NMR (500 MHz, DMSO-d_6): δ 7.94 (br d, *J* = 8.5 Hz, 1H), 7.58 (d, *J* = 8.5 Hz, 1H), 7.51 (br d, *J* = 8.2 Hz, 1H), 7.34−7.29 (m, 3H), 7.29−7.20 (m, 2H), 4.07−3.88 (m, 1H), 3.18−2.98 (m, 1H), 2.95−2.82 (m, 1H), 2.63 (br d, *J* = 16.2 Hz, 1H), 2.38−2.20 (m, 1H), 2.03−1.81 (m, 5H), 1.26 (m, 1H). ESI-MS: *m*/*z* 572.01 ([M + H$^+$]). HPLC: t_R = 2.14 min.

(*R*)-*N*-((3*R*,3a*S*,9b*S*)-9b-((4-Fluorophenyl)sulfonyl)-7-(perfluoropropan-2-yl)-2,3,3a,4,5,9b-hexahydro-1*H*-cyclopenta[*a*]naphthalen-3-yl)-2-hydroxypropanamide (3c, Table 1). A procedure similar to that described in the synthesis of **3b** was used to prepare **3c** from **14** and (*R*)-2-hydroxypropanoic acid. ^{1}H NMR (500 MHz, DMSO-d_6): δ 7.89 (br d, *J* = 8.2 Hz, 1H), 7.60−7.49 (m, 2H), 7.36−7.23 (m, 5H), 4.05−3.90 (m, 2H), 3.63−3.40 (m, 1H), 3.07−2.94 (m, 1H), 2.87 (br d, *J* = 8.2 Hz, 1H), 2.64 (br d, *J* = 16.2 Hz, 1H), 2.56−2.53 (m, 3H), 2.38−2.21 (m, 1H), 2.03−1.89 (m, 3H), 1.87−1.65 (m, 1H), 1.30−1.18 (m, 5H), 1.00 (m, 1H). ESI-MS: *m*/*z* 586.13 ([M + H$^+$]). HPLC: t_R = 2.10 min.

***N*-((3*R*,3a*S*,9b*S*)-9b-((4-Fluorophenyl)sulfonyl)-7-(perfluoropropan-2-yl)-2,3,3a,4,5,9b-hexahydro-1*H*-cyclopenta[*a*]naphthalen-3-yl)-2-hydroxy-2-methylpropanamide (3d, Table 1).** A procedure similar to that described in the synthesis of **3b** was used to prepare **3d** from **14** and 2-hydroxy-2-methylpropanoic acid. ^{1}H NMR (500 MHz, DMSO-d_6): δ 7.83 (br d, *J* = 8.2 Hz, 1H), 7.59 (br d, *J* = 8.5 Hz, 1H), 7.52 (br d, *J* = 8.2 Hz, 1H), 7.35−7.30 (m, 3H), 7.30−7.22 (m, 2H), 3.98 (br t, *J* = 7.3 Hz, 1H), 3.07−2.96 (m, 1H), 2.87 (br d, *J* = 7.9 Hz, 1H), 2.65 (br d, *J* = 15.9 Hz, 1H), 2.34−2.19 (m, 1H), 2.03−1.90 (m, 3H), 1.89−1.72 (m, 1H), 1.28 (br d, *J* = 14.0 Hz, 6H). ^{13}C NMR (126 MHz, methanol-d_4): δ 179.56 (s, 1C), 167.62 (d, *J* = 256.1 Hz, 1C), 143.98 (d, *J* = 1.8 Hz, 1C), 138.08 (s, 1C), 134.44 (d, *J* = 9.1 Hz, 2C), 132.98 (d, *J* = 2.7 Hz, 1C), 132.68 (d, *J* = 1.8 Hz, 1C), 127.68 (d, *J* = 20.0 Hz, 1C), 126.32 (d, *J* = 10.0 Hz, 1C), 124.61−124.49 (m, 1C), 125.93−118.12 (m, 2C), 116.93 (d, *J* = 22.7 Hz, 2C), 94.28−91.30 (m, 1C), 77.17 (s, 1C), 73.86 (s, 1C), 57.85 (s, 1C), 48.92 (s, 1C), 35.66 (s, 1C), 32.23 (s, 1C), 29.40 (s, 1C), 28.23 (s, 1C), 27.96 (s, 1C), 27.84 (s, 1C). RHMS (ESI) *m*/*z*: calcd for $C_{26}H_{26}F_8NO_4S$ [M + H$^+$], 600.1449; found, 600.1449.

https://dx.doi.org/10.1021/acs.jmedchem.0c01992
J. Med. Chem. 2021, 64, 2714−2724

HPLC: t_R = 2.23 min. Co-crystal structure of **3d** (BMS-986313) with the LBD of RORγt (pdb id: 7KQJ).

***N*-((3*R*,3a*S*,9b*S*)-9b-((4-Fluorophenyl)sulfonyl)-7-(perfluoropropan-2-yl)-2,3,3a,4,5,9b-hexahydro-1*H*-cyclopenta[*a*]naphthalen-3-yl)-2-hydroxy-N,2-dimethylpropanamide (3d-Me, Figure 2).** ^{1}H NMR (500 MHz, chloroform-*d*): δ 7.63 (d, *J* = 8.5 Hz, 1H), 7.49 (d, *J* = 8.2 Hz, 1H), 7.26−7.07 (m, 3H), 6.94 (t, *J* = 8.2 Hz, 2H), 3.36−3.28 (m, 1H), 3.07 (br d, *J* = 5.7 Hz, 1H), 2.93−2.86 (m, 2H), 2.61 (s, 3H), 2.56−2.41 (m, 1H), 2.06−1.84 (m, 5H), 1.76 (ddd, *J* = 15.9, 12.7, 3.6 Hz, 3H), 1.37−1.17 (m, 6H). ESI-MS: *m*/*z* 614.5 ([M + H$^+$]). HPLC: t_R = 1.11 min. BEH C18 2.1 × 50 mm 1.7 u; mobile phase A: 100% water with 0.05% TFA; mobile phase B: 100% acetonitrile with 0.05% TFA; gradient: initial 98% A to 2% B, and then 2% A to 98% B over 1.8 min, then a 0.75 min hold at 100% B; flow rate: 0.8 mL/min.

***N*-((3*R*,3a*S*,9b*S*)-9b-((4-Fluorophenyl)sulfonyl)-7-(perfluoropropan-2-yl)-2,3,3a,4,5,9b-hexahydro-1*H*-cyclopenta[*a*]naphthalen-3-yl)-3-hydroxy-3-methylbutanamide (3e, Table 1).** A procedure similar to that described in the synthesis of **3b** was used to prepare **3e** from **14** and 3-hydroxy-3-methylbutanoic acid. ^{1}H NMR (500 MHz, DMSO-d_6): δ 8.13 (br d, *J* = 7.9 Hz, 1H), 7.52−7.42 (m, 2H), 7.36 (s, 1H), 7.32−7.25 (m, 4H), 4.81 (s, 1H), 4.06−3.90 (m, 1H), 3.06−2.93 (m, 1H), 2.80 (br d, *J* = 6.1 Hz, 1H), 2.72−2.61 (m, 1H), 2.30−2.19 (m, 3H), 2.09−1.99 (m, 2H), 1.96 (br d, *J* = 5.2 Hz, 1H), 1.89−1.74 (m, 1H), 1.29 (br d, *J* = 10.1 Hz, 1H), 1.18 (s, 6H). ESI-MS: *m*/*z* 614.26 ([M + H$^+$]). HPLC: t_R = 2.28 min.

***N*-((3*R*,3a*S*,9b*S*)-9b-((4-Fluorophenyl)sulfonyl)-7-(perfluoropropan-2-yl)-2,3,3a,4,5,9b-hexahydro-1*H*-cyclopenta[*a*]naphthalen-3-yl)-1-hydroxycyclohexane-1-carboxamide (3f, Table 1).** A procedure similar to that described in the synthesis of **3b** was used to prepare **3f** from **14** and 1-hydroxycyclohexane-1-carboxylic acid. ^{1}H NMR (500 MHz, DMSO-d_6): δ 7.87 (br d, *J* = 8.5 Hz, 1H), 7.59 (d, *J* = 8.2 Hz, 1H), 7.52 (br d, *J* = 8.2 Hz, 1H), 7.35−7.22 (m, 5H), 5.17 (s, 1H), 3.98 (br t, *J* = 7.5 Hz, 1H), 3.18 (d, *J* = 5.2 Hz, 1H), 3.06−2.94 (m, 1H), 2.94−2.80 (m, 1H), 2.74−2.60 (m, 1H), 2.28 (br dd, *J* = 13.9, 8.4 Hz, 1H), 2.07−1.88 (m, 3H), 1.86−1.76 (m, 1H), 1.74−1.64 (m, 2H), 1.62−1.43 (m, 7H), 1.31−1.13 (m, 2H). ESI-MS: *m*/*z* 640.30 ([M + H$^+$]). HPLC: t_R = 2.38 min.

***N*-((3*R*,3a*S*,9b*S*)-9b-((4-Fluorophenyl)sulfonyl)-7-(perfluoropropan-2-yl)-2,3,3a,4,5,9b-hexahydro-1*H*-cyclopenta[*a*]naphthalen-3-yl)-4-hydroxytetrahydro-2*H*-pyran-4-carboxamide (3g, Table 1).** A procedure similar to that described in the synthesis of **3b** was used to prepare **3g** from **14** and 4-hydroxytetrahydro-2*H*-pyran-4-carboxylic acid. ^{1}H NMR (500 MHz, DMSO-d_6): δ 7.97 (br d, *J* = 8.5 Hz, 1H), 7.59 (d, *J* = 8.5 Hz, 1H), 7.52 (br d, *J* = 8.5 Hz, 1H), 7.34−7.22 (m, 5H), 3.98 (br t, *J* = 7.5 Hz, 1H), 3.72−3.59 (m, 2H), 3.09−2.97 (m, 1H), 2.93−2.82 (m, 1H), 2.73−2.59 (m, 1H), 2.44−2.24 (m, 1H), 2.02−1.88 (m, 6H), 1.87−1.73 (m, 1H), 1.47−1.33 (m, 2H), 1.25 (m, 1H). ESI-MS: *m*/*z* 642.29 ([M + H$^+$]). HPLC: t_R = 2.22 min.

2-Amino-*N*-((3*R*,3a*S*,9b*S*)-9b-((4-fluorophenyl)sulfonyl)-7-(perfluoropropan-2-yl)-2,3,3a,4,5,9b-hexahydro-1*H*-cyclopenta[*a*]naphthalen-3-yl)-2-methylpropanamide (4a, Table 1). To a solution of **14** (40 mg, 0.078 mmol), 2-((*tert*-butoxycarbonyl)amino)-2-methylpropanoic acid (20.58 mg, 0.101 mmol), HATU (38.5 mg, 0.101 mmol) in DMF (2 mL) was added triethylamine (32.6 μL, 0.234 mmol). The reaction mixture was stirred at rt for 3 h before water (10 mL) was added. The resulting mixture was basified with 1N NaOH solution (3 mL) and extracted with ethyl acetate (10 × 2 mL), and the combined ethyl acetate extracts were dried over Na_2SO_4 and concentrated under rotary evaporation. The crude material was dissolved in CH_2Cl_2 (2 mL) followed by TFA (1.5 mL). The reaction mixture was stirred at rt for 1 h before water (10 mL) was added. The resulting mixture was extracted with ethyl acetate (10 × 2 mL) and the combined ethyl acetate extracts were dried over Na_2SO_4 and concentrated under rotary evaporation. The crude material was purified by preparative HPLC [Xbridge C18 19 × 200 mm, 5 μm (Waters Corp.); mobile phase A: 5:95 MeCN/water with 10 μM ammonium acetate; mobile phase B: 95:5 MeCN/water with 10 mM ammonium acetate; flow rate 20 mL/min; gradient: 29−69% B over 20 min, then a 4-min hold at 100% B] to give **4a** (31.7 mg, 68% yield). ^{1}H NMR (500 MHz, DMSO-d_6): δ 8.27 (br d, *J* = 7.4 Hz, 1H), 7.54−7.34 (m, 3H), 7.33−7.23 (m, 3H), 3.99 (br t, *J* = 7.8 Hz, 1H), 3.54−3.36 (m, 2H), 3.12−2.93 (m, 1H), 2.69 (br d, *J* = 16.1 Hz, 1H), 2.33−2.16 (m, 1H), 2.08−1.89 (m, 2H), 1.53 (br d, *J* = 12.8 Hz, 6H), 1.45 (br s, 2H). ESI-MS: *m*/*z* 599.12 ([M + H$^+$]). HPLC: t_R = 1.89 min.

3-Amino-*N*-((3*R*,3a*S*,9b*S*)-9b-((4-fluorophenyl)sulfonyl)-7-(perfluoropropan-2-yl)-2,3,3a,4,5,9b-hexahydro-1*H*-cyclopenta[*a*]naphthalen-3-yl)-3-methylbutanamide (4b, Table 1). A procedure similar to that described in the synthesis of **4a** was used to prepare **4b** from **14** and 3-((*tert*-butoxycarbonyl)-amino)-3-methylbutanoic acid. ^{1}H NMR (500 MHz, DMSO-d_6): δ 8.48 (br d, *J* = 7.9 Hz, 1H), 7.53−7.40 (m, 2H), 7.37 (s, 1H), 7.28 (d, *J* = 6.7 Hz, 3H), 4.13−3.94 (m, 1H), 3.09−2.94 (m, 1H), 2.90−2.75 (m, 1H), 2.68 (br d, *J* = 15.0 Hz, 1H), 2.33−2.20 (m, 3H), 2.11−2.01 (m, 2H), 1.98 (br d, *J* = 5.5 Hz, 1H), 1.92−1.81 (m, 3H), 1.35−1.21 (m, 2H), 1.18 (s, 6H). ESI-MS: *m*/*z* 613.13 ([M + H$^+$]). HPLC: t_R = 1.88 min.

***N*-((3*R*,3a*S*,9b*S*)-9b-((4-Fluorophenyl)sulfonyl)-7-(perfluoropropan-2-yl)-2,3,3a,4,5,9b-hexahydro-1*H*-cyclopenta[*a*]naphthalen-3-yl)-4-hydroxypiperidine-4-carboxamide (4c, Table 1).** A procedure similar to that described in the synthesis of **4a** was used to prepare **4c** from **14** and 1-(*tert*-butoxycarbonyl)-4-hydroxypiperidine-4-carboxylic acid. ^{1}H NMR (500 MHz, DMSO-d_6): δ 8.00 (br d, *J* = 8.5 Hz, 1H), 7.59 (br d, *J* = 8.5 Hz, 1H), 7.52 (br d, *J* = 8.2 Hz, 1H), 7.32 (br s, 3H), 7.30−7.21 (m, 2H), 3.98 (br t, *J* = 7.6 Hz, 1H), 3.18 (s, 1H), 3.09−2.95 (m, 1H), 2.91 (br s, 1H), 2.86 (br s, 3H), 2.75−2.59 (m, 1H), 2.38−2.22 (m, 1H), 2.00−1.82 (m, 8H), 1.80 (br s, 1H), 1.57−1.37 (m, 2H), 1.26 (br d, *J* = 9.5 Hz, 1H), 1.00 (d, *J* = 6.4 Hz, 1H). ESI-MS: *m*/*z* 641.18 ([M + H$^+$]). HPLC: t_R = 1.80 min.

***N*-((3*R*,3a*S*,9b*S*)-9b-((4-Fluorophenyl)sulfonyl)-7-(perfluoropropan-2-yl)-2,3,3a,4,5,9b-hexahydro-1*H*-cyclopenta[*a*]naphthalen-3-yl)-2-methyl-2-(piperazin-1-yl)propanamideide (4d, Table 1).** A procedure similar to that described in the synthesis of **4a** was used to prepare **4d** from **14** and 2-(4-(*tert*-butoxycarbonyl)-piperazin-1-yl)-2-methylpropanoic acid. ^{1}H NMR (500 MHz, DMSO-d_6): δ 8.24−8.06 (m, *J* = 8.2 Hz, 1H), 7.59 (br d, *J* = 8.5 Hz, 1H), 7.55−7.42 (m, *J* = 8.2 Hz, 1H), 7.33−7.18 (m, 4H), 4.05−3.94 (m, 1H), 3.58−3.43 (m, 3H), 3.18 (br s, 1H), 3.08−2.87 (m, 2H), 2.70 (br s, 1H), 2.68−2.60 (m, 3H), 2.42−2.22 (m, 1H), 2.22−2.01 (m, 1H), 1.99−1.88 (m, 2H), 1.88−1.71 (m, 1H), 1.18 (s, 3H), 1.13 (s, 3H). ESI-MS: *m*/*z* 668.32 ([M + H$^+$]). HPLC: t_R = 1.92 min.

***N*-((3*R*,3a*S*,9b*S*)-9b-((4-Fluorophenyl)sulfonyl)-7-(perfluoropropan-2-yl)-2,3,3a,4,5,9b-hexahydro-1*H*-cyclopenta[*a*]naphthalen-3-yl)-2-methyl-2-morpholinopropanamide (4e, Table 1).** A procedure similar to that described in the synthesis of **3b** was used to prepare **4e** from **9** and 2-methyl-2-morpholinopropanoic acid. ^{1}H NMR (500 MHz, DMSO-d_6): δ 7.96 (br d, *J* = 8.4 Hz, 1H), 7.60 (d, *J* = 8.4 Hz, 1H), 7.51 (br d, *J* = 8.4 Hz, 1H), 7.34−7.20 (m, 5H), 4.14−3.96 (m, 1H), 3.71 (t, *J* = 4.4 Hz, 3H), 3.07−2.94 (m, 1H), 2.94−2.81 (m, 1H), 2.65 (br d, *J* = 16.2 Hz, 1H), 2.46−2.40 (m, 2H), 2.39−2.22 (m, 1H), 2.06 (br dd, *J* = 13.4, 4.8 Hz, 1H), 2.01−1.90 (m, 2H), 1.80 (br dd, *J* = 12.5, 7.5 Hz, 1H), 1.36−1.21 (m, 2H), 1.17 (s, 3H), 1.12 (s, 3H). ESI-MS: *m*/*z* 669.14 ([M + H$^+$]). HPLC: t_R = 1.98 min.

2-Acetamido-*N*-((3*R*,3a*S*,9b*S*)-9b-((4-fluorophenyl)sulfonyl)-7-(perfluoropropan-2-yl)-2,3,3a,4,5,9b-hexahydro-1*H*-cyclopenta[*a*]naphthalen-3-yl)acetamide (5a, Table 1). A procedure similar to that described in the synthesis of **3b** was used to prepare **5a** from **14** and acetyl glycine. ^{1}H NMR (500 MHz, DMSO-d_6): δ 7.95 (br d, *J* = 7.4 Hz, 2H), 7.54−7.43 (m, 2H), 7.36−7.21 (m, 5H), 4.04−3.85 (m, 1H), 3.71 (d, *J* = 5.7 Hz, 2H), 3.13−2.93 (m, 1H), 2.92−2.78 (m, 1H), 2.72−2.60 (m, 1H), 2.24 (br dd, *J* = 14.4, 7.3 Hz, 1H), 2.10−1.92 (m, 3H), 1.92−1.82 (m, 4H), 1.30 (m, 1H). ESI-MS: *m*/*z* 613.28 ([M + H$^+$]). HPLC: t_R = 2.10 min.

1-Acetyl-*N*-((3*R*,3a*S*,9b*S*)-9b-((4-fluorophenyl)sulfonyl)-7-(perfluoropropan-2-yl)-2,3,3a,4,5,9b-hexahydro-1*H*-cyclopenta[*a*]naphthalen-3-yl)piperidine-4-carboxamide (5b, Table 1). A procedure similar to that described in the synthesis of **3b** was used to prepare **5b** from **14** and 1-acetylpiperidine-4-carboxylic

https://dx.doi.org/10.1021/acs.jmedchem.0c01992
J. Med. Chem. 2021, 64, 2714−2724

acid. ^{1}H NMR (500 MHz, DMSO-d_6): δ 8.07 (br d, J = 7.9 Hz, 1H), 7.52−7.43 (m, 2H), 7.35 (s, 1H), 7.28 (br d, J = 7.0 Hz, 4H), 4.36 (br d, J = 11.0 Hz, 1H), 3.96−3.87 (m, 1H), 3.83 (br d, J = 11.6 Hz, 1H), 3.08−2.96 (m, 2H), 2.81 (br d, J = 6.4 Hz, 1H), 2.65 (br d, J = 15.6 Hz, 1H), 2.48−2.34 (m, 1H), 2.29−2.11 (m, 1H), 2.07−1.90 (m, 6H), 1.84−1.64 (m, 3H), 1.52 (br d, J = 12.2 Hz, 1H), 1.38 (br d, J = 11.9 Hz, 1H), 1.24 (m, 1H). ESI-MS: m/z 667.55 ([M + H$^+$]). HPLC: t_R = 2.15 min.

(*S*)-1-(2-Cyanoethyl)-*N*-((3*R*,3a*S*,9b*S*)-9b-((4-fluorophenyl)-sulfonyl)-7-(perfluoropropan-2-yl)-2,3,3a,4,5,9b-hexahydro-1*H*-cyclopenta[*a*]naphthalen-3-yl)-5-oxopyrrolidine-2-carboxamide (5c, Table 1). A procedure similar to that described in the synthesis of **3b** was used to prepare **5c** from **14** and (*S*)-1-(2-cyanoethyl)-5-oxopyrrolidine-2-carboxylic acid.[25] ^{1}H NMR (500 MHz, DMSO-d_6): δ 8.55 (br d, J = 7.6 Hz, 1H), 7.50−7.39 (m, 2H), 7.34 (s, 1H), 7.25 (d, J = 7.0 Hz, 4H), 4.27 (br dd, J = 7.5, 3.2 Hz, 1H), 4.01−3.91 (m, 1H), 3.81−3.63 (m, 1H), 3.50 (br d, J = 8.5 Hz, 1H), 3.17 (d, J = 5.2 Hz, 1H), 3.03 (br dd, J = 13.6, 6.6 Hz, 2H), 2.90 (br d, J = 8.9 Hz, 1H), 2.81−2.70 (m, 2H), 2.65 (br d, J = 15.9 Hz, 1H), 2.41−2.20 (m, 4H), 2.08 (br dd, J = 13.6, 5.6 Hz, 1H), 2.03−1.94 (m, 2H), 1.93−1.80 (m, 2H), 1.25 (br d, J = 10.1 Hz, 1H). ESI-MS: m/z 678.45 ([M + H$^+$]). HPLC: t_R = 2.15 min.

(2*S*,4*R*)-4-Fluoro-*N*-((3*R*,3a*S*,9b*S*)-9b-((4-fluorophenyl)-sulfonyl)-7-(perfluoropropan-2-yl)-2,3,3a,4,5,9b-hexahydro-1*H*-cyclopenta[*a*]naphthalen-3-yl)-1-(methyl-d_3)-5-oxopyrrolidine-2-carboxamide (5d, Table 1). A procedure similar to that described in the synthesis of **3b** was used to prepare **5d** from **14** and **11**[25] (Scheme 1). ^{1}H NMR (500 MHz, DMSO-d_6): δ 8.73 (br d, J = 7.6 Hz, 1H), 7.51−7.37 (m, 2H), 7.34 (br s, 1H), 7.25 (br d, J = 7.0 Hz, 4H), 5.29 (t, J = 7.6 Hz, 1H), 5.18 (t, J = 7.5 Hz, 1H), 4.21 (br d, J = 8.5 Hz, 1H), 4.06−3.91 (m, 1H), 3.17 (s, 1H), 3.03 (td, J = 7.2, 4.3 Hz, 1H), 2.92−2.76 (m, 1H), 2.73−2.59 (m, 1H), 2.48−2.32 (m, 1H), 2.32−2.18 (m, 1H), 2.10−1.95 (m, 3H), 1.95−1.84 (m, 2H), 1.24 (m, 1H). ESI-MS: m/z 659.96 ([M + H$^+$]). HPLC: t_R = 2.20 min.

(2*S*,4*R*)-*N*-((3*R*,3a*S*,9b*S*)-9b-((4-Fluorophenyl)sulfonyl)-7-(perfluoropropan-2-yl)-2,3,3a,4,5,9b-hexahydro-1*H*-cyclopenta[*a*]naphthalen-3-yl)-4-hydroxy-1-(methyl-d_3)-5-oxopyrrolidine-2-carboxamide (5e, Table 1). A procedure similar to that described in the synthesis of **3b** was used to prepare **5e** from **14** and (2*S*,4*R*)-4-hydroxy-1-(methyl-d_3)-5-oxopyrrolidine-2-carboxylic acid.[25] ^{1}H NMR (500 MHz, DMSO-d_6): δ 8.56 (br d, J = 7.6 Hz, 1H), 7.52−7.40 (m, 2H), 7.35 (s, 1H), 7.27 (br d, J = 6.7 Hz, 3H), 4.21 (m, 1H), 4.06 (br d, J = 7.9 Hz, 1H), 4.00−3.92 (m, 1H), 3.09−2.96 (m, 1H), 2.92−2.84 (m, 2H), 2.74 (s, 1H), 2.66 (br d, J = 15.0 Hz, 1H), 2.30−2.11 (m, 2H), 2.07−1.85 (m, 4H), 1.26 (m, 1H). ESI-MS: m/z 658.10 ([M + H$^+$]). HPLC: t_R = 2.12 min.

***N*-((3*R*,3a*S*,9b*S*)-9b-((4-Fluorophenyl)sulfonyl)-7-(perfluoropropan-2-yl)-2,3,3a,4,5,9b-hexahydro-1*H*-cyclopenta[*a*]naphthalen-3-yl)methanesulfonamide (6a, Table 1).** A procedure similar to that described in the synthesis of **3a** was used to prepare **6a** from **14** and methanesulfonyl chloride. ^{1}H NMR (500 MHz, DMSO-d_6): δ 7.53−7.41 (m, 3H), 7.38−7.25 (m, 4H), 3.52 (br s, 1H), 3.18 (d, J = 4.9 Hz, 1H), 3.00 (br dd, J = 13.9, 7.2 Hz, 1H), 2.92 (s, 3H), 2.86−2.74 (m, 1H), 2.70−2.59 (m, 1H), 2.20−2.02 (m, 3H), 1.96−1.79 (m, 1H), 1.43−1.23 (m, 1H). ESI-MS: m/z 592.02 ([M + H$^+$]). HPLC: t_R = 2.21 min.

***N*-((3*R*,3a*S*,9b*S*)-9b-((4-Fluorophenyl)sulfonyl)-7-(perfluoropropan-2-yl)-2,3,3a,4,5,9b-hexahydro-1*H*-cyclopenta[*a*]naphthalen-3-yl)-2-sulfamoylacetamide (6b, Table 1).** A procedure similar to that described in the synthesis of **3b** was used to prepare **6b** from **14** and 2-sulfamoylacetic acid. ^{1}H NMR (500 MHz, DMSO-d_6): δ 8.49 (br d, J = 7.9 Hz, 1H), 7.51−7.37 (m, 2H), 7.34 (s, 1H), 7.30−7.21 (m, 4H), 4.03−3.87 (m, 2H), 3.81−3.62 (m, 2H), 3.03 (br dd, J = 14.8, 6.3 Hz, 1H), 2.81 (br d, J = 6.4 Hz, 1H), 2.63 (br d, J = 15.9 Hz, 1H), 2.32−2.18 (m, 1H), 2.12−2.02 (m, 1H), 2.02−1.94 (m, 2H), 1.86 (br dd, J = 10.5, 8.1 Hz, 1H), 1.32−1.16 (m, 1H). ESI-MS: m/z 634.88 ([M + H$^+$]). HPLC: t_R = 1.99 min.

***N*-((3*R*,3a*S*,9b*S*)-9b-((4-Fluorophenyl)sulfonyl)-7-(perfluoropropan-2-yl)-2,3,3a,4,5,9b-hexahydro-1*H*-cyclopenta[*a*]naphthalen-3-yl)-4-hydroxy-1-(methylsulfonyl)piperidine-4-carboxamide (6c, Table 1).** A procedure similar to that described in the synthesis of **3b** was used to prepare **6c** from **14** and 4-hydroxy-1-(methylsulfonyl)piperidine-4-carboxylic acid, HCl. ^{1}H NMR (500 MHz, DMSO-d_6): δ 8.04 (br d, J = 8.2 Hz, 1H), 7.59 (d, J = 8.5 Hz, 1H), 7.52 (br d, J = 8.2 Hz, 1H), 7.35−7.23 (m, 5H), 4.04−3.94 (m, 1H), 3.90 (s, 1H), 3.46 (br s, 1H), 3.05−2.87 (m, 6H), 2.65 (br d, J = 15.9 Hz, 1H), 2.38−2.23 (m, 1H), 2.02−1.82 (m, 6H), 1.70−1.57 (m, 2H), 1.37−1.20 (m, 1H). ESI-MS: m/z 719.47 ([M + H$^+$]). HPLC: t_R = 2.2 min.

***N*-((3*R*,3a*S*,9b*S*)-9b-((4-Fluorophenyl)sulfonyl)-7-(perfluoropropan-2-yl)-2,3,3a,4,5,9b-hexahydro-1*H*-cyclopenta[*a*]naphthalen-3-yl)tetrahydro-2*H*-thiopyran-4-carboxamide 1,1-Dioxide (6d, Table 1).** A procedure similar to that described in the synthesis of **3b** was used to prepare **6d** from **14** and tetrahydro-2*H*-thiopyran-4-carboxylic acid 1,1-dioxide. ^{1}H NMR (500 MHz, DMSO-d_6): δ 8.23 (br d, J = 7.6 Hz, 1H), 7.52−7.40 (m, 2H), 7.33 (s, 1H), 7.25 (br d, J = 6.1 Hz, 4H), 4.04−3.85 (m, 1H), 3.62 (m, 1H), 3.19−3.08 (m, 4H), 3.01 (td, J = 7.1, 4.1 Hz, 1H), 2.82 (br d, J = 6.7 Hz, 1H), 2.70−2.58 (m, 1H), 2.29−2.19 (m, 1H), 2.17−2.10 (m, 1H), 2.10−1.90 (m, 6H), 1.87−1.68 (m, 1H), 1.22 (s, 2H), 1.00 (d, J = 6.4 Hz, 1H). ESI-MS: m/z 674.03 ([M + H$^+$]). HPLC: t_R = 2.14 min.

***N*-((3*R*,3a*S*,9b*S*)-9b-((4-Fluorophenyl)sulfonyl)-7-(perfluoropropan-2-yl)-2,3,3a,4,5,9b-hexahydro-1*H*-cyclopenta[*a*]naphthalen-3-yl)-4-hydroxytetrahydro-2*H*-thiopyran-4-carboxamide 1,1-Dioxide (6e, Table 1).** A procedure similar to that described in the synthesis of **3b** was used to prepare **6e** from **14** and 4-hydroxytetrahydro-2*H*-thiopyran-4-carboxylic acid 1,1-dioxide. ^{1}H NMR (500 MHz, DMSO-d_6): δ 8.14 (br d, J = 8.2 Hz, 1H), 7.63−7.56 (m, J = 8.5 Hz, 1H), 7.56−7.49 (m, J = 8.5 Hz, 1H), 7.36−7.23 (m, 5H), 3.99 (br t, J = 7.5 Hz, 1H), 3.11−2.99 (m, 3H), 2.93 (br d, J = 9.2 Hz, 1H), 2.76−2.59 (m, 1H), 2.48−2.27 (m, 3H), 2.05−1.83 (m, 6H), 1.26 (br d, J = 9.8 Hz, 1H). ESI-MS: m/z 690.43 ([M + H$^+$]). HPLC: t_R = 2.15 min.

(1*R*,4*r*)-4-(((3*R*,3a*S*,9b*S*)-9b-((4-Fluorophenyl)sulfonyl)-7-(perfluoropropan-2-yl)-2,3,3a,4,5,9b-hexahydro-1*H*-cyclopenta[*a*]naphthalen-3-yl)carbamoyl)cyclohexane-1-carboxylic Acid (6f, Table 1). A procedure similar to that described in the synthesis of **3b** was used to prepare **6f** from **14** and (1*r*,4*r*)-cyclohexane-1,4-dicarboxylic acid. ^{1}H NMR (500 MHz, DMSO-d_6): δ 8.01 (br d, J = 7.9 Hz, 1H), 7.47 (s, 2H), 7.33 (s, 1H), 7.31−7.23 (m, 4H), 3.89 (br t, J = 7.6 Hz, 1H), 3.75−3.54 (m, 2H), 3.00 (br dd, J = 13.0, 5.6 Hz, 1H), 2.79 (br d, J = 6.1 Hz, 1H), 2.70−2.58 (m, 1H), 2.24−2.08 (m, 3H), 2.06−1.89 (m, 5H), 1.86−1.66 (m, 3H), 1.42−1.20 (m, 5H). ESI-MS: m/z 668.07 ([M + H$^+$]). HPLC: t_R = 1.93 min.

1-((3*R*,3a*S*,9b*S*)-9b-((4-Fluorophenyl)sulfonyl)-7-(perfluoropropan-2-yl)-2,3,3a,4,5,9b-hexahydro-1*H*-cyclopenta[*a*]naphthalen-3-yl)-3-methylurea (7a, Table 1). To a solution of **14** (70 mg, 0.136 mmol) in CH_2Cl_2 (3 mL) was added phosgene (79 μL, 0.150 mmol) at 0 °C followed by triethylamine (76 μL, 0.545 mmol) and stirred at 0 °C for 0.5 h, and then warmed to rt for 0.5 h. The solution was removed on the rotavapor, and the solid was dissolved in CH_2Cl_2 (2 mL) followed by the addition of methenamine (6.35 mg, 0.205 mmol), triethylamine (76 μL, 0.545 mmol), and stirred at rt for 2 h. The reaction mixture was diluted with water, sat $NaHCO_3$ solution, and extracted with EtOAc. The organic layer was collected and concentrated on a rotavapor to give the crude product, which was then purified by preparative HPLC [Xbridge C18 19 × 200 mm, 5 μm (Waters Corp.); mobile phase A: 5:95 MeCN/water with 10 mM ammonium acetate; mobile phase B: 95:5 MeCN/water with 10 mM ammonium acetate; flow rate 20 mL/min; gradient: increasing B, then isocratic at 100% B] to give **7a** (18.5 mg, 24% yield). ^{1}H NMR (500 MHz, DMSO-d_6): δ 7.52−7.40 (m, 2H), 7.34−7.18 (m, 4H), 6.12 (br d, J = 8.2 Hz, 1H), 5.72 (br d, J = 3 9 Hz, 1H), 3.93−3.73 (m, 1H), 3.00 (br dd, J = 13.7, 6.8 Hz, 1H), 2.73−2.60 (m, 2H), 2.27−2.10 (m, 1H), 2.08−2.00 (m, 3H), 1.95 (br d, J = 8.6 Hz, 1H), 1.77−1.67 (m, 1H), 1.34−1.15 (m, 2H). ESI-MS: m/z 571.21 ([M + H$^+$]). HPLC: t_R = 2.13 min.

1-((3*R*,3a*S*,9b*S*)-9b-((4-Fluorophenyl)sulfonyl)-7-(perfluoropropan-2-yl)-2,3,3a,4,5,9b-hexahydro-1*H*-cyclopenta[*a*]naphthalen-3-yl)-3-(2-hydroxyethyl)urea (7b, Table 1). A

https://dx.doi.org/10.1021/acs.jmedchem.0c01992
J. Med. Chem. 2021, 64, 2714−2724

procedure similar to that described in the synthesis of **7a** was used to prepare **7b** from **14**, phosgene, and 2-aminoethan-1-ol. ^{1}H NMR (500 MHz, DMSO-d_6): δ 7.46 (s, 2H), 7.34−7.19 (m, 5H), 6.23 (br d, J = 8.2 Hz, 1H), 5.87 (br t, J = 5.1 Hz, 1H), 3.95−3.79 (m, 1H), 3.51−3.45 (m, 14H), 3.43 (br s, 1H), 3.09 (q, J = 5.6 Hz, 2H), 3.01 (br dd, J = 13.7, 6.3 Hz, 1H), 2.72−2.59 (m, 2H), 2.18 (dt, J = 11.1, 7.2 Hz, 1H), 2.09−1.99 (m, 2H), 1.96 (br d, J = 4.9 Hz, 1H), 1.82−1.67 (m, 1H), 1.36−1.18 (m, 2H). ESI-MS: m/z 601.19 ([M + H$^+$]). HPLC: t_R = 2.02 min.

1-((3*R*,3a*S*,9b*S*)-9b-((4-Fluorophenyl)sulfonyl)-7-(perfluoropropan-2-yl)-2,3,3a,4,5,9b-hexahydro-1*H*-cyclopenta[*a*]naphthalen-3-yl)-3-(2-hydroxy-2-methylpropyl)urea (7c, Table 1). A procedure similar to that described in the synthesis of **7a** was used to prepare **7c** from **14**, phosgene, and 1-amino-2-methylpropan-2-ol. ^{1}H NMR (500 MHz, DMSO-d_6): δ 7.51−7.44 (m, 2H), 7.33 (s, 1H), 7.30−7.23 (m, 4H), 6.38 (br d, J = 8.5 Hz, 1H), 5.88 (br t, J = 5.6 Hz, 1H), 4.54 (s, 1H), 3.90−3.79 (m, 1H), 3.48 (br d, J = 5.5 Hz, 1H), 3.05−2.89 (m, 3H), 2.70−2.59 (m, 2H), 2.24−2.13 (m, 1H), 2.09−1.90 (m, 3H), 1.74 (br dd, J = 10.2, 8.1 Hz, 1H), 1.27 (br d, J = 10.7 Hz, 1H), 1.05 (s, 6H). ESI-MS: m/z 629.17 ([M + H$^+$]). HPLC: t_R = 2.16 min.

2-Hydroxy-2-methylpropyl ((3*R*,3a*S*,9b*S*)-9b-((4-Fluorophenyl)sulfonyl)-7-(perfluoropropan-2-yl)-2,3,3a,4,5,9b-hexahydro-1*H*-cyclopenta[*a*]naphthalen-3-yl)-carbamate (7d, Table 1). A procedure similar to that described in the synthesis of **7a** was used to prepare **7d** from **14**, phosgene, and 2-methylpropane-1,2-diol. ^{1}H NMR (500 MHz, DMSO-d_6): δ 7.55−7.47 (m, 2H), 7.43 (br d, J = 7.6 Hz, 1H), 7.37−7.25 (m, 5H), 3.75 (s, 2H), 3.72−3.54 (m, 1H), 3.08−2.93 (m, 1H), 2.85 (br d, J = 6.7 Hz, 1H), 2.73−2.59 (m, 1H), 2.21 (ddd, J = 14.3, 11.0, 7.0 Hz, 1H), 2.06−1.91 (m, 3H), 1.87−1.76 (m, 1H), 1.35−1.19 (m, 2H), 1.12 (s, 6H). ESI-MS: m/z 630.25 ([M + H$^+$]). HPLC: t_R = 2.29 min.

Biological Methods. All procedures involving animals were reviewed and approved by the Institutional Animal Care and Use Committee and conformed to the "Guide for the Care and Use of Laboratory Animals" published by the National Institutes of Health (NIH publication no. 85−23, revised 2011). Detailed biological experimental procedures, animal studies, and assay conditions used in this study can be found in our recent publications, refs 20. and 21.

■ ASSOCIATED CONTENT

Supporting Information

The Supporting Information is available free of charge at https://pubs.acs.org/doi/10.1021/acs.jmedchem.0c01992.

Molecular formula strings (CSV)

SMILES representation of compounds with key data; PDB ID 7KQJ for compound **3d**, analytic experimental HPLC methods; synthesis of compound **5d**; synthetic procedures and analytical data of **8**−**14**; synthesis of intermediates **16**, **21**, and compounds **3**−**7**; HPLC traces of compound **3d**; biological experimental procedures of the RORγt Gal4 Luc reporter gene assay, RORγt hWB IL17 assay protocol, and RORγt mouse whole blood IL17 assay protocol; and in vivo experimental protocols of the IMQ-induced model of skin inflammation and IL23-induced mouse model of acanthosis (PDF)

■ AUTHOR INFORMATION

Corresponding Authors

Michael G. Yang − *Research and Early Development, Bristol Myers Squibb Company, Princeton, New Jersey 08543-4000, United States;* orcid.org/0000-0003-2908-4060; Phone: 609-252-3234; Email: michael.yang@bms.com

T. G. Murali Dhar − *Research and Early Development, Bristol Myers Squibb Company, Princeton, New Jersey 08543-4000, United States;* orcid.org/0000-0003-0738-1021; Phone: 609-252-4158; Email: murali.dhar@bms.com

Authors

Myra Beaudoin-Bertrand − *Research and Early Development, Bristol Myers Squibb Company, Princeton, New Jersey 08543-4000, United States*

Zili Xiao − *Research and Early Development, Bristol Myers Squibb Company, Princeton, New Jersey 08543-4000, United States*

David Marcoux − *Research and Early Development, Bristol Myers Squibb Company, Princeton, New Jersey 08543-4000, United States;* orcid.org/0000-0002-0295-7717

Carolyn A. Weigelt − *Research and Early Development, Bristol Myers Squibb Company, Princeton, New Jersey 08543-4000, United States*

Shiuhang Yip − *Research and Early Development, Bristol Myers Squibb Company, Princeton, New Jersey 08543-4000, United States*

Dauh-Rurng Wu − *Research and Early Development, Bristol Myers Squibb Company, Princeton, New Jersey 08543-4000, United States*

Max Ruzanov − *Research and Early Development, Bristol Myers Squibb Company, Princeton, New Jersey 08543-4000, United States*

John S. Sack − *Research and Early Development, Bristol Myers Squibb Company, Princeton, New Jersey 08543-4000, United States*

Jinhong Wang − *Research and Early Development, Bristol Myers Squibb Company, Princeton, New Jersey 08543-4000, United States*

Melissa Yarde − *Research and Early Development, Bristol Myers Squibb Company, Princeton, New Jersey 08543-4000, United States*

Sha Li − *Research and Early Development, Bristol Myers Squibb Company, Princeton, New Jersey 08543-4000, United States*

David J. Shuster − *Research and Early Development, Bristol Myers Squibb Company, Princeton, New Jersey 08543-4000, United States*

Jenny H. Xie − *Research and Early Development, Bristol Myers Squibb Company, Princeton, New Jersey 08543-4000, United States*

Tara Sherry − *Research and Early Development, Bristol Myers Squibb Company, Princeton, New Jersey 08543-4000, United States*

Mary T. Obermeier − *Research and Early Development, Bristol Myers Squibb Company, Princeton, New Jersey 08543-4000, United States*

Aberra Fura − *Research and Early Development, Bristol Myers Squibb Company, Princeton, New Jersey 08543-4000, United States*

Kevin Stefanski − *Research and Early Development, Bristol Myers Squibb Company, Princeton, New Jersey 08543-4000, United States*

Georgia Cornelius − *Research and Early Development, Bristol Myers Squibb Company, Princeton, New Jersey 08543-4000, United States*

Purnima Khandelwal − *Research and Early Development, Bristol Myers Squibb Company, Princeton, New Jersey 08543-4000, United States*

Ananta Karmakar − *Department of Discovery Synthesis, Biocon Bristol-Myers Squibb Research Centre, Bengaluru 560099, India;* orcid.org/0000-0003-3795-5807
Mushkin Basha − *Department of Discovery Synthesis, Biocon Bristol-Myers Squibb Research Centre, Bengaluru 560099, India*
Venkatesh Babu − *Department of Discovery Synthesis, Biocon Bristol-Myers Squibb Research Centre, Bengaluru 560099, India*
Arun Kumar Gupta − *Department of Discovery Synthesis, Biocon Bristol-Myers Squibb Research Centre, Bengaluru 560099, India*
Arvind Mathur − *Research and Early Development, Bristol Myers Squibb Company, Princeton, New Jersey 08543-4000, United States*
Luisa Salter-Cid − *Research and Early Development, Bristol Myers Squibb Company, Princeton, New Jersey 08543-4000, United States*
Rex Denton − *Research and Early Development, Bristol Myers Squibb Company, Princeton, New Jersey 08543-4000, United States*
Qihong Zhao − *Research and Early Development, Bristol Myers Squibb Company, Princeton, New Jersey 08543-4000, United States*

Complete contact information is available at: https://pubs.acs.org/10.1021/acs.jmedchem.0c01992

Notes

The authors declare no competing financial interest.

■ ACKNOWLEDGMENTS

The authors would like to thank Qingjie Liu for providing intermediate **11** and Douglas Batt for thorough review of the manuscript.

■ ABBREVIATIONS

AUC, area under the curve; bid, twice a day; Boc, butyloxycarbonyl; CL, clearance; compd, compound; F, bioavailability; hWB, human whole blood; IL, interleukin; KO, knock-out; LM, liver microsome; MetStab, metabolic stability; PD, pharmacodynamics; PK, pharmacokinetic; ROR, retinoid-related orphan receptor; SAR, structure activity relationship; SFC, supercritical fluid chromatography; Th17, T helper 17 cells; THF, tetrahydrofuran; V_{ss}, volume of distribution

■ REFERENCES

(1) (a) Huh, J. R.; Littman, D. R. Small molecule inhibitors of RORγt: Targeting Th17 cells and other applications. *Eur. J. Immunol.* **2012**, *42*, 2232−2237. (b) Zhang, Y.; Luo, X.-y.; Wu, D.-h.; Xu, Y. ROR nuclear receptors: structures, related diseases, and drug discovery. *Acta Pharmacol. Sin.* **2015**, *36*, 71−87. (c) Aranda, A.; Pascual, A. Nuclear hormone receptors and gene expression. *Physiol. Rev.* **2001**, *81*, 1269−1304.

(2) (a) Eberl, G.; Marmon, S.; Sunshine, M.-J.; Rennert, P. D.; Choi, Y.; Littman, D. R. An essential function for the nuclear receptor RORγt in the generation of fetal lymphoid tissue inducer cells. *Nat. Immunol.* **2004**, *5*, 64−73. (b) Ivanov, I. I.; McKenzie, B. S.; Zhou, L.; Tadokoro, C. E.; Lepelley, A.; Lafaille, J. J.; Cua, D. J.; Littman, D. R. The Orphan Nuclear Receptor RORγt Directs the Differentiation Program of Proinflammatory IL-17+ T Helper Cells. *Cell* **2006**, *126*, 1121−1133.

(3) Scoville, S. D.; Mundy-Bosse, B. L.; Zhang, M. H.; Carson, W. E., III; Caligiuri, M. A.; Freud, A. G. A progenitor cell expressing transcription factor RORγt generates all human innate lymphoid cell subsets. *Immunity* **2016**, *44*, 1140−1150.

(4) (a) Sano, T.; Huang, W.; Hall, J. A.; Yang, Y.; Chen, A.; Gavzy, S. J.; Lee, J.-Y.; Ziel, J. W.; Miraldi, E. R.; Domingos, A. I.; Bonneau, R.; Littman, D. R. An IL-23R/IL-22 circuit regulates epithelial serum amyloid A to promote local effector Th17 responses. *Cell* **2015**, *163*, 381−393. (b) Tanaka, K.; Martinez, G. J.; Yan, X.; Long, W.; Ichiyama, K.; Chi, X.; Kim, B.-S.; Reynolds, J. M.; Chung, Y.; Tanaka, S.; Liao, L.; Nakanishi, Y.; Yoshimura, A.; Zheng, P.; Wang, X.; Tian, Q.; Xu, J.; O'Malley, B. W.; Dong, C. Regulation of pathogenic T helper 17 cell differentiation by steroid receptor coactivator-3. *Cell Rep.* **2018**, *23*, 2318−2329.

(5) (a) Gaffen, S. L.; Jain, R.; Garg, A. V.; Cua, D. J. The IL-23-IL-17 immune axis: from mechanisms to therapeutic testing. *Nat. Rev. Immunol.* **2014**, *14*, 585−600. (b) Ivanov, I. I.; McKenzie, B. S.; Zhou, L.; Tadokoro, C. E.; Lepelley, A.; Lafaille, J. J.; Cua, D. J.; Littman, D. R. The Orphan Nuclear Receptor RORγt Directs the Differentiation Program of Proinflammatory IL-17+ T Helper Cells. *Cell* **2006**, *126*, 1121−1133.

(6) Baliwag, J.; Barnes, D. H.; Johnston, A. Cytokines in psoriasis. *Cytokine* **2015**, *73*, 342−350.

(7) (a) Langley, R. G.; Elewski, B. E.; Lebwohl, M.; Reich, K.; Griffiths, C. E. M.; Papp, K.; Puig, L.; Nakagawa, H.; Spelman, L.; Sigurgeirsson, B.; Rivas, E.; Tsai, T.-F.; Wasel, N.; Tyring, S.; Salko, T.; Hampele, I.; Notter, M.; Karpov, A.; Helou, S.; Papavassilis, C. Secukinumab in Plaque Psoriasis - Results of Two Phase 3 Trials. *N. Engl. J. Med.* **2014**, *371*, 326−338. (b) Papp, K. A.; Leonardi, C.; Menter, A.; Ortonne, J.-P.; Krueger, J. G.; Kricorian, G.; Aras, G.; Li, J.; Russell, C. B.; Thompson, E. H. Z.; Baumgartner, S. Brodalumab, an Anti-Interleukin-17-Receptor Antibody for Psoriasis. *N. Engl. J. Med.* **2012**, *366*, 1181−1189.

(8) Leonardi, C.; Matheson, R.; Zachariae, C.; Cameron, G.; Li, L.; Edson-Heredia, E.; Braun, D.; Banerjee, S. Anti-Interleukin-17 Monoclonal Antibody Ixekizumab in Chronic Plaque Psoriasis. *N. Engl. J. Med.* **2012**, *366*, 1190−1199.

(9) Gege, C. RORγt inhibitors as potential back-ups for the phase II candidate VTP-43742 from Vitae Pharmaceuticals: patent evaluation of WO2016061160 and US20160122345. *Expert Opin. Ther. Pat.* **2017**, *27*, 1−8.

(10) Leppkes, M.; Becker, C.; Ivanov, I. I.; Hirth, S.; Wirtz, S.; Neufert, C.; Pouly, S.; Murphy, A. J.; Valenzuela, D. M.; Yancopoulos, G. D.; Becher, B.; Littman, D. R.; Neurath, M. F. RORgamma-expressing Th17 cells induce murine chronic intestinal inflammation via redundant effects of IL-17A and IL-17F. *Gastroenterology* **2009**, *136*, 257−267.

(11) Korn, T.; Bettelli, E.; Oukka, M.; Kuchroo, V. K. IL-17 and Th17 Cells. *Annu. Rev. Immunol.* **2009**, *27*, 485−517.

(12) Cho, J. H. The genetics and immunopathogenesis of inflammatory bowel disease. *Nat. Rev. Immunol.* **2008**, *8*, 458−466.

(13) Duerr, R. H.; Taylor, K. D.; Brant, S. R.; Rioux, J. D.; Silverberg, M. S.; Daly, M. J.; Steinhart, A. H.; Abraham, C.; Regueiro, M.; Griffiths, A.; Dassopoulos, T.; Bitton, A.; Yang, H.; Targan, S.; Datta, L. W.; Kistner, E. O.; Schumm, L. P.; Lee, A. T.; Gregersen, P. K.; Barmada, M. M.; Rotter, J. I.; Nicolae, D. L.; Cho, J. H. A genome-wide association study identifies IL23R as an inflammatory bowel disease gene. *Science* **2006**, *314*, 1461−1463.

(14) Huh, J. R.; Leung, M. W. L.; Huang, P.; Ryan, D. A.; Krout, M. R.; Malapaka, R. R. V.; Chow, J.; Manel, N.; Ciofani, M.; Kim, S. V.; Cuesta, A.; Santori, F. R.; Lafaille, J. J.; Xu, H. E.; Gin, D. Y.; Rastinejad, F.; Littman, D. R. Digoxin and its derivatives suppress TH17 cell differentiation by antagonizing RORγt activity. *Nature* **2011**, *472*, 486−490.

(15) Kojetin, D. J.; Burris, T. P. REV-ERB and ROR nuclear receptors as drug targets. *Nat. Rev. Drug Discovery* **2014**, *13*, 197−216.

(16) Solt, L. A.; Kumar, N.; Nuhant, P.; Wang, Y.; Lauer, J. L.; Liu, J.; Istrate, M. A.; Kamenecka, T. M.; Roush, W. R.; Vidović, D.; Schürer, S. C.; Xu, J.; Wagoner, G.; Drew, P. D.; Griffin, P. R.; Burris, T. P. Suppression of TH17 differentiation and autoimmunity by a synthetic ROR ligand. *Nature* **2011**, *472*, 491−494.

(17) Zhuang, L.. Discovery of VTP-43742, a RORct inverse agonist for the treatment of psoriasis. *Presented at the 13th winter conference on medicinal and bioorganic chemistry*; Steamboat Springs, CO., January 22−26, 2017.
(18) Fauber, B. P.; Magnuson, S. Modulators of the nuclear receptor retinoic acid receptor-related orphan receptor-γ (RORγ or RORc). *J. Med. Chem.* **2014**, *57*, 5871−5892.
(19) (a) Duan, J. J.-W.; Lu, Z.; Jiang, B.; Stachura, S.; Weigelt, C. A.; Sack, J. S.; Khan, J.; Ruzanov, M.; Galella, M. A.; Wu, D.-R.; Yarde, M.; Shen, D.-R.; Shuster, D. J.; Borowski, V.; Xie, J. H.; Zhang, L.; Vanteru, S.; Gupta, A. K.; Mathur, A.; Zhao, Q.; Foster, W.; Salter-Cid, L. M.; Carter, P. H.; Dhar, T. G. M. Structure-based Discovery of Phenyl (3-Phenylpyrrolidin-3-yl)sulfones as Selective, Orally Active RORγt Inverse Agonists. *ACS Med. Chem. Lett.* **2019**, *10*, 367−373. (b) Lu, Z.; Duan, J. J.-W.; Xiao, H.; Neels, J.; Wu, D.-R.; Weigelt, C. A.; Sack, J. S.; Khan, J.; Ruzanov, M.; An, Y.; Yarde, M.; Karmakar, A.; Vishwakrishnan, S.; Baratam, V.; Shankarappa, H.; Vanteru, S.; Babu, V.; Basha, M.; Kumar Gupta, A.; Kumaravel, S.; Mathur, A.; Zhao, Q.; Salter-Cid, L. M.; Carter, P. H.; Murali Dhar, T. G. Identification of potent, selective and orally bioavailable phenyl ((R)-3-phenyl-pyrrolidin-3-yl)sulfone analogues as RORγt inverse agonists. *Bioorg. Med. Chem. Lett.* **2019**, *29*, 2265−2269.
(20) Marcoux, D.; Duan, J. J.-W.; Shi, Q.; Cherney, R. J.; Srivastava, A. S.; Cornelius, L.; Batt, D. G.; Liu, Q.; Beaudoin-Bertrand, M.; Weigelt, C. A.; Khandelwal, P.; Vishwakrishnan, S.; Selvakumar, K.; Karmakar, A.; Gupta, A. K.; Basha, M.; Ramlingam, S.; Manjunath, N.; Vanteru, S.; Karmakar, S.; Maddala, N.; Vetrichelvan, M.; Gupta, A.; Rampulla, R. A.; Mathur, A.; Yip, S.; Li, P.; Wu, D.-R.; Khan, J.; Ruzanov, M.; Sack, J. S.; Wang, J.; Yarde, M.; Cvijic, M. E.; Li, S.; Shuster, D. J.; Borowski, V.; Xie, J. H.; McIntyre, K. W.; Obermeier, M. T.; Fura, A.; Stefanski, K.; Cornelius, G.; Hynes, J.; Tino, J. A.; Macor, J. E.; Salter-Cid, L.; Denton, R.; Zhao, Q.; Carter, P. H.; Dhar, T. G. M. Rationally Designed, Conformationally Constrained Inverse Agonists of RORγt-Identification of a Potent, Selective Series with Biologic-Like in Vivo Efficacy. *J. Med. Chem.* **2019**, *62*, 9931−9946.
(21) Cherney, R. J.; Cornelius, L. A. M.; Srivastava, A.; Weigelt, C. A.; Marcoux, D.; Duan, J. J.-W.; Shi, Q.; Batt, D. G.; Liu, Q.; Yip, S.; Wu, D.-R.; Ruzanov, M.; Sack, J.; Khan, J.; Wang, J.; Yarde, M.; Cvijic, M. E.; Mathur, A.; Li, S.; Shuster, D.; Khandelwal, P.; Borowski, V.; Xie, J.; Obermeier, M.; Fura, A.; Stefanski, K.; Cornelius, G.; Tino, J. A.; Macor, J. E.; Salter-Cid, L.; Denton, R.; Zhao, Q.; Carter, P. H.; Dhar, T. G. M. Discovery of BMS-986251: A Clinically Viable, Potent, and Selective RORγt Inverse Agonist. *ACS Med. Chem. Lett.* **2020**, *11*, 1221−1227.
(22) Marcoux, D.; Bertrand, M. B.; Weigelt, C. A.; Yip, S.; Galella, M.; Park, H.; Wu, D.-R.; Wang, J.; Yarde, M.; Cvijic, M. E.; Li, S.; Hynes, J.; Tino, J. A.; Zhao, Q.; Dhar, T. G. M. Annulation reaction enables the identification of an exocyclic amide tricyclic chemotype as retinoic acid Receptor-Related orphan receptor gamma (RORγ/RORc) inverse agonists. *Bioorg. Med. Chem. Lett.* **2020**, *30*, 127466.
(23) Liu, Q.; Batt, D. G.; Weigelt, C. A.; Yip, S.; Wu, D.-R.; Ruzanov, M.; Sack, J. S.; Wang, J.; Yarde, M.; Li, S.; Shuster, D. J.; Xie, J. H.; Sherry, T.; Obermeier, M. T.; Fura, A.; Stefanski, K.; Cornelius, G.; Khandelwal, P.; Tino, J. A.; Macor, J. E.; Salter-Cid, L.; Denton, R.; Zhao, Q.; Dhar, T. G. M. Novel Tricyclic Pyroglutamide Derivatives as Potent RORγt Inverse Agonists Identified using a Virtual Screening Approach. *ACS Med. Chem. Lett.* **2020**, *11*, 2510−2518.
(24) Metabolic stability is defined as the percentage of parent compound remaining over 10 min of incubation time in the presence of human, rat and mouse liver microsomes, respectively. The initial compound concentration was 0.5 μM; protein concentration 1 mg/mL.
(25) The synthetic procedures and analytical data of 8−14 (Scheme 1) are described in the following patent: Marcoux, D.; Bertrand, M. B.; Dhar, T. G. M.; Yang, M. G.; Xiao, Z.; Xiao, H. T.; Zhu, Y.; Weigelt, C. A.; Batt, D. G. Tricyclic sulfones as ROR gamma modulators. U.S. Patent 10,435,369 B2.

https://dx.doi.org/10.1021/acs.jmedchem.0c01992
J. Med. Chem. 2021, 64, 2714−2724